AIP | Journal of Applied Physics

Amorphization and reduction of thermal conductivity in porous silicon by irradiation with swift heavy ions

Pascal J. Newby, Bruno Canut, Jean-Marie Bluet, Séverine Gomès, Mykola Isaiev et al.

Citation: J. Appl. Phys. **114**, 014903 (2013); doi: 10.1063/1.4812280
View online: http://dx.doi.org/10.1063/1.4812280
View Table of Contents: http://jap.aip.org/resource/1/JAPIAU/v114/i1
Published by the AIP Publishing LLC.

JOURNAL OF APPLIED PHYSICS **114**, 014903 (2013)

Amorphization and reduction of thermal conductivity in porous silicon by irradiation with swift heavy ions

Pascal J. Newby,[1,2,a)] Bruno Canut,[1] Jean-Marie Bluet,[1] Séverine Gomès,[3] Mykola Isaiev,[4] Roman Burbelo,[4] Konstantinos Termentzidis,[5] Patrice Chantrenne,[6] Luc G. Fréchette,[2] and Vladimir Lysenko[1]

[1]*Institut des Nanotechnologies de Lyon, Université de Lyon, INL-UMR5270, CNRS, INSA de Lyon, Villeurbanne 69621, France*
[2]*Institut Interdisciplinaire d'Innovation Technologique (3IT), Université de Sherbrooke, CNRS UMI-LN2, Sherbrooke, Québec J1K0A5, Canada*
[3]*Centre de Thermique de Lyon, Université de Lyon, CETHIL-UMR5008, CNRS, INSA de Lyon, Villeurbanne 69621, France*
[4]*Faculty of Physics, Taras Shevchenko National University of Kyiv, 64/13, Volodymyrs'ka St., Kyiv 01601, Ukraine*
[5]*Laboratoire LEMTA, Université de Lorraine-CNRS UMR 7563, 54506 Vandœuvre-lès-Nancy cedex, France*
[6]*Université de Lyon, INSA de Lyon, MATEIS-UMR CNRS 5510, Villeurbanne 69621, France*

(Received 19 April 2013; accepted 10 June 2013; published online 3 July 2013)

In this article, we demonstrate that the thermal conductivity of nanostructured porous silicon is reduced by amorphization and also that this amorphous phase in porous silicon can be created by swift (high-energy) heavy ion irradiation. Porous silicon samples with 41%-75% porosity are irradiated with 110 MeV uranium ions at six different fluences. Structural characterisation by micro-Raman spectroscopy and SEM imaging show that swift heavy ion irradiation causes the creation of an amorphous phase in porous Si but without suppressing its porous structure. We demonstrate that the amorphization of porous silicon is caused by electronic-regime interactions, which is the first time such an effect is obtained in crystalline silicon with single-ion species. Furthermore, the impact on the thermal conductivity of porous silicon is studied by micro-Raman spectroscopy and scanning thermal microscopy. The creation of an amorphous phase in porous silicon leads to a reduction of its thermal conductivity, up to a factor of 3 compared to the non-irradiated sample. Therefore, this technique could be used to enhance the thermal insulation properties of porous Si. Finally, we show that this treatment can be combined with pre-oxidation at 300 °C, which is known to lower the thermal conductivity of porous Si, in order to obtain an even greater reduction. [http://dx.doi.org/10.1063/1.4812280]

I. INTRODUCTION

Crystalline silicon is the material of choice for fabrication in the majority of MEMS (micro-electro-mechanical systems) and sensors. It has a high thermal conductivity, λ, of 156 $W\,m^{-1}\,K^{-1}$,[1] which is ideal for electronic applications, but makes it unsuitable for devices that require thermal insulation, such as micro-bolometers or flowmeters, for example. Alternative materials with low thermal conductivity exist, but silicon remains preferable to benefit from the vast array of microfabrication processes which have been developed for it. A possible approach to bridge this compromise is to reduce the thermal conductivity of silicon where needed by making it porous.

Indeed, porous silicon (PSi), made by electrochemical etching of single crystal silicon wafers (c-Si), has a thermal conductivity which is 2–3 orders of magnitude lower than that of bulk c-Si.[2,3] This is due to its porosity and percolation, but also to phonon scattering on the surface of pores and increased phonon-phonon scattering caused by its nanoscale structure.[4] Its low thermal conductivity, combined with easy fabrication on silicon substrates, make PSi a good material for thermal insulation in MEMS and sensors.[3,5]

Thermal conductivity of PSi decreases cubically as its porosity, P, is increased.[2] However, there is a limit to the reduction in thermal conductivity which can be obtained by increasing porosity, as porosification also has a detrimental effect on the mechanical properties of PSi.[6] Indeed, measurements of its hardness have shown a $(1–P)^{2/3}$ dependance up to 75% porosity, and a sharper decrease beyond this.[7] When drying PSi, the surface-tension caused by evaporation of water in the pores is enough to induce cracking in high porosity films.[8] A compromise must therefore be found between thermal conductivity and mechanical performance. Thermal conductivity of PSi can also be reduced by creating a very thin SiO_2 layer, by oxidising it for 1 h at 300 °C. The maximum reduction of thermal conductivity which can be achieved by this method is by a factor of two.[9,10] Further oxidation is not useful as, besides causing swelling and stress in the PSi layer which can lead to cracking or wafer warpage in extreme cases,[11,12] the thermal conductivity will actually increase again beyond this point.[9,10] Consequently, alternative techniques for reducing the thermal conductivity of PSi without increasing its porosity or damaging it are desirable and could lead to a broader adoption of PSi as a thermal insulation material in MEMS.

a)Electronic mail: Pascal.Newby@USherbrooke.ca.

The thermal conductivity of c-Si can also be reduced by amorphizing it. In general, disorder in crystalline solids reduces thermal transport,[13] as seen in amorphous silicon (a-Si) with $\lambda = 1$–$5\,\mathrm{W\,m^{-1}\,K^{-1}}$, depending on the fabrication process.[14]

We propose to combine these two approaches, in order to gain an even greater reduction of thermal conductivity, i.e., by first electrochemically etching c-Si to create a nanoscale porosity, and then rendering the remaining silicon amorphous. In this work, we will propose ion-irradiation as the method for amorphizing silicon.

Ion irradiation of bulk crystalline silicon with low to medium-energy ions (<0.1 MeV per atomic mass unit) is dominated by collisions between the incoming ions and the target atoms, which induces atomic displacements responsible for damage creation and even amorphization at high irradiation fluences. This is known as the "nuclear regime."[15] However, this method is not suitable for amorphizing porous silicon. Indeed, a previous study on the irradiation of PSi in the nuclear regime showed that irradiation with 4 MeV $^4He^+$ ions caused a densification of the porous layer,[16] i.e., the layer was damaged and its porosity reduced (thus increasing thermal conductivity).

Higher energy irradiation with heavy ions (>0.1 MeV per atomic mass unit) leads to interaction in the so-called "electronic regime." In this regime, the incoming ions excite the electrons in the target, and very localised melting around the path of the ion can occur, depending on the type of material. Swift (i.e., high energy) heavy ion irradiation of most covalent insulating materials and certain binary semiconductors causes the creation of a cylindrical damaged zone ("latent track") along the path of the ions.[17,18] In the case of bulk c-Si, this has only been achieved with 30-40 MeV C_{60} clusters,[19] which leave an amorphous silicon track along their path. Otherwise c-Si is known to be generally insensitive to damage in this regime,[17] especially when irradiated with single-ion species. In the case of porous silicon, irradiation with swift heavy ions has also been carried out in order to improve its photoluminescence efficiency,[20–22] but these studies lacked a structural analysis of the irradiation-induced effects, so the effect of electronic-regime interaction between swift heavy ions and PSi is still unknown.

In this work, we propose to leverage the electronic-regime interactions caused by swift heavy-ion irradiation to amorphize porous silicon and therefore reduce its thermal conductivity. Given the confinement provided by the porous nanostructures and their low electrical conductivity,[23] PSi should be more sensitive than bulk Si to electronic-regime interactions caused by swift heavy-ion irradiation, and an amorphous phase could be created in this way.

In this article, we show that high energy ion irradiation of electrochemically etched porous silicon can be used to amorphize it in a controlled manner, but without suppressing its porous structure. The creation of an amorphous phase leads to a reduction of the thermal conductivity of PSi, so this technique could be used to enhance the thermal insulation properties of PSi. We have studied the effects of irradiation on the structure and morphology of PSi, and on its thermal conductivity. We also irradiated lightly oxidised PSi, to show that the thermal conductivity reduction can be combined with that caused by irradiation. The structural characterisation methods used were micro-Raman spectroscopy and SEM imaging, while thermal conductivity was evaluated by Raman spectroscopy and scanning thermal microscopy (SThM).

II. EXPERIMENTAL DETAILS

A. Sample preparation

Porous silicon samples were formed by electrochemical etching of p+ monocrystalline (100) Si wafers ($\rho = 0.01$–$0.02\ \Omega$ cm). This was carried out in a Teflon cell, using a (1:1) 48% hydrofluoric acid and anhydrous ethanol mixture. A pulsed current was used, with zero-current etch-stop periods to improve uniformity of the PSi layers.[24] Their thickness was 10 μm, and three different porosities were used: 41%, 56%, and 75%. This parameter was controlled via the anodisation current density. Additional information regarding the anodisation process can be found in Ref. 25. PSi fabricated in this way is mesoporous and formed of dendritic silicon quasi-columns, with a diameter on the order of 10 nm, perpendicular to the wafer surface, and separated by pores. These quasi-columns remain monocrystalline and retain the crystalline orientation of the substrate (the SEM images of non-irradiated PSi presented later in Fig. 4 are good examples of typical mesoporous Si).

Certain 56% porosity samples were lightly oxidised before irradiation at 300 °C in dry O_2 for 1 h.[9,10] Irradiation of the PSi samples was carried out at the IRRSUD beamline of the GANIL accelerator[26] with 110 MeV uranium ions. Six different fluences were tested between 1×10^{12} and $7 \times 10^{13}\,\mathrm{cm^{-2}}$.

B. Structural characterisation techniques

The creation of an amorphous phase within the PSi layers was studied, both qualitatively and quantitatively, by Raman spectroscopy. These measurements were done on the surface, using micro-Raman equipment at a laser wavelength of 532 nm. The morphology of PSi was studied by SEM imaging on the cross-section of cleaved samples.

C. Thermal conductivity measurement techniques

Thermal conductivity measurements were carried out with two different techniques. The first technique used was a scanning thermal microscopy (SThM) technique based on atomic force microscopy (AFM). A thermoresistive wire probe was mounted on the AFM cantilever and was used in its active mode and in DC regime. The probe was heated by Joule effect and used to locally deliver heat to the sample. The electrical power required for maintaining the probe's temperature constant while it contacts the sample depends on the sample's thermal conductivity. This was exploited for determining λ after calibration with samples of well-known thermal conductivity.[27]

The second technique is based on micro-Raman spectroscopy and involves measuring the shift of the silicon transverse-optical (TO) peak, which depends on the temperature of the sample. The material is heated with a 532 nm laser and the local temperature is monitored. For a given

absorbed laser power, the surface of a material with lower thermal conductivity will reach higher temperatures and thus a larger Raman shift. A simple analytical model for calculating thermal conductivity using the variation of Raman shift versus laser power has previously been published,[10,28] with an error of 30%.[29] However, to apply this model, the layer being studied should be semi-infinite compared to the diameter of the laser beam, whereas in our measurements, the laser beam diameter was 1.5 μm and the PSi layer was only 10 μm thick. Therefore, we have further developed this analytical model to account for the influence of the silicon substrate beneath the PSi layers. This model is presented in detail in Appendix B.

III. STRUCTURAL CHARACTERISATION RESULTS

A. Characterisation of amorphous phase

1. Qualitative measurements

Raman spectroscopy measurements were carried out on the PSi samples. Figure 1 shows the evolution of the Raman measurements as a function of irradiation fluence for 56% porosity PSi. As irradiation fluence increases, it is clearly visible that an amorphous Si peak appears at 480 cm^{-1} and increases relative to the crystalline silicon peak (around 520 cm^{-1}), whereas the c-Si peak gradually disappears. The peak at 480 cm^{-1} is characteristic of amorphous silicon[30] and the response of the transverse optical (TO) branch. This demonstrates that ion-irradiation caused amorphization of porous silicon. Amorphization was observed in the same way after irradiation of 41% and 75% porosity PSi samples.

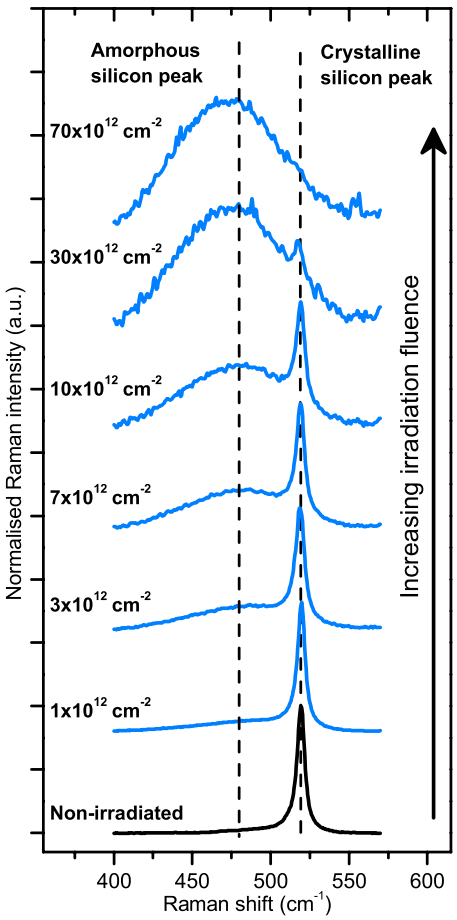

FIG. 1. Raman spectra of 56% porosity PSi for different irradiation fluence levels. Each spectrum is normalised to the intensity of its highest peak. The relative intensity of the amorphous phase increases with the irradiation fluence.

2. Amorphous volume fraction measurements

The Raman spectra were processed to extract the amorphous volume fraction, ρ_a, created in the PSi layer by irradiation. This was achieved by first separating the PSi and a-Si contributions, and then integrating the intensity of each peak, as illustrated in Fig. 2, to obtain the integrated intensities of the crystalline and amorphous phases, I_c and I_a. The volume fraction of the amorphous phase, ρ_a, is given by the ratio $\rho_a = I_a/(I_c + I_a)$. The details of this procedure are given in Appendix A.

Figure 3 shows the amorphous volume fraction versus irradiation fluence for 41%, 56%, and 75% porosity PSi, extracted from the Raman spectra. These data confirm quantitatively that the volume fraction of the amorphous phase increased with irradiation fluence. The 56% and 75% porosity samples both became totally amorphous at the highest fluence. We can also observe that at a given fluence, the amorphous fraction increased with porosity.

B. Change of morphology

As micro-Raman spectroscopy gives macroscopic information on amorphization, SEM imaging was performed to observe the microscopic effect of ion irradiation on the porous silicon structure. Cross-section SEM images of 56% and 75% porosity PSi, after irradiation at different fluences are presented in Fig. 4. There was no detectable change of morphology up to high levels of amorphization, with reorganisation beginning above 83% amorphous fraction for 56% porosity, and between 68% and 83% amorphous fraction for 75% porosity. Beyond this, there was a partial reorganisation, with a coarsening of the PSi structure, but the samples remained porous, even at 100% amorphization. Images were taken at the top, middle, and bottom of each sample, and we observed no visible difference between the structural reorganisation, so we conclude that amorphization took place throughout the depth of the PSi layer. It is worth

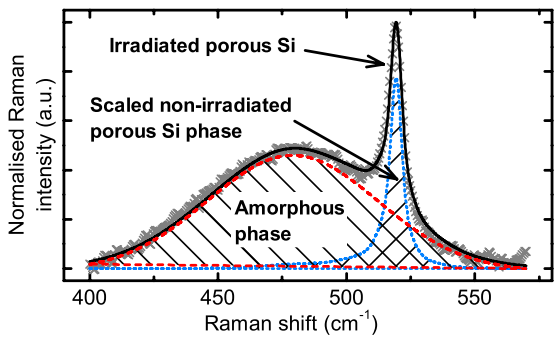

FIG. 2. Extraction of the contribution of the amorphous phase created by irradiation in Raman spectra (here 56% porosity PSi irradiated at 1×10^{13} cm^{-2}): the scaled non-irradiated PSi phase (dotted line) and a Gaussian curve at 480 cm^{-1} (dashed line) are fitted to the experimental spectrum (crosses) to obtain a fitted spectrum (solid line).

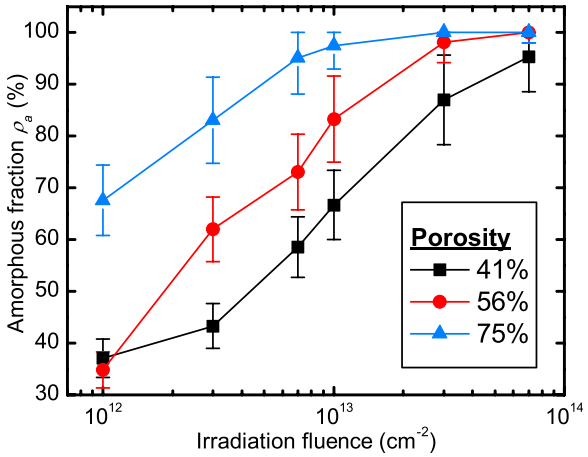

FIG. 3. Amorphous fraction versus irradiation fluence for 41%, 56%, and 75% porosity PSi samples. The amorphous fraction increases with the fluence before reaching a plateau at 100%.

mentioning that the PSi samples remained otherwise intact after irradiation, and there was no visible damage, i.e., cracking or crushing of the structure.

C. Discussion on amorphization by ion irradiation

We have demonstrated that by irradiating porous silicon with swift heavy ions, we can create an amorphous phase in PSi. The degree of amorphization can be controlled with the irradiation fluence, and the porous morphology is not destroyed: at high amorphization levels there is a partial reorganisation of the structure, but it remains porous.

It is remarkable that the PSi skeleton remained unchanged up to at least $\rho_a = 83\%$ and $\rho_a = 68\%$ for, respectively, 56% and 75% porosity, and was only partially reorganised at 100% amorphization. Indeed, as a comparison, low energy irradiation with 4 MeV $^4He^+$ causes a densification of the porous layer,[16] i.e., destruction of the porous structure, which is clearly not the case here, despite much higher energy and heavier species being used. So what exactly are the mechanisms involved? We stated in the introduction that there are two different regimes for interaction between the ions and the target: nuclear and electronic. The predominance of each regime depends on the ion's energy. Figure 5 shows the stopping power (the energy per length unit transferred from the ion to the target) of uranium ions in a silicon target as a function of energy, for both the nuclear and electronic contributions, calculated using SRIM software.[31] As we can see, at the energy level used in this study (110 MeV), electronic slowing-down is predominant. Whereas interaction in the nuclear regime would have caused collisional damage and thus densification of the porous layer, electronic-regime interaction simply leaves an amorphous track along the path of the ions. This explains the partial amorphization of PSi without destroying the porous structure which we observed.

The projected range R_p of the ions (the distance travelled inside the target) was also calculated with SRIM to be 14 μm for 110 MeV uranium ions in bulk silicon. The density of the target material is one of the principal parameters used for calculating R_p, so a basic estimation of R_p in PSi can be made by replacing the density of bulk silicon with the effective density of PSi. In this way, we calculated $R_p = 57$ μm for 75% porosity PSi. This means that the ions cross the PSi layers (which are 10 μm thick) and stop in the bulk substrate beneath. Nuclear interactions only become dominant at depths close to R_p, so the whole PSi layer should be amorphized, which is consistent with our observation from the SEM images, that structural modification, when it occurred, was observed across the layer.

So electronic-regime interactions are responsible for the amorphization of porous silicon. However, we mentioned in

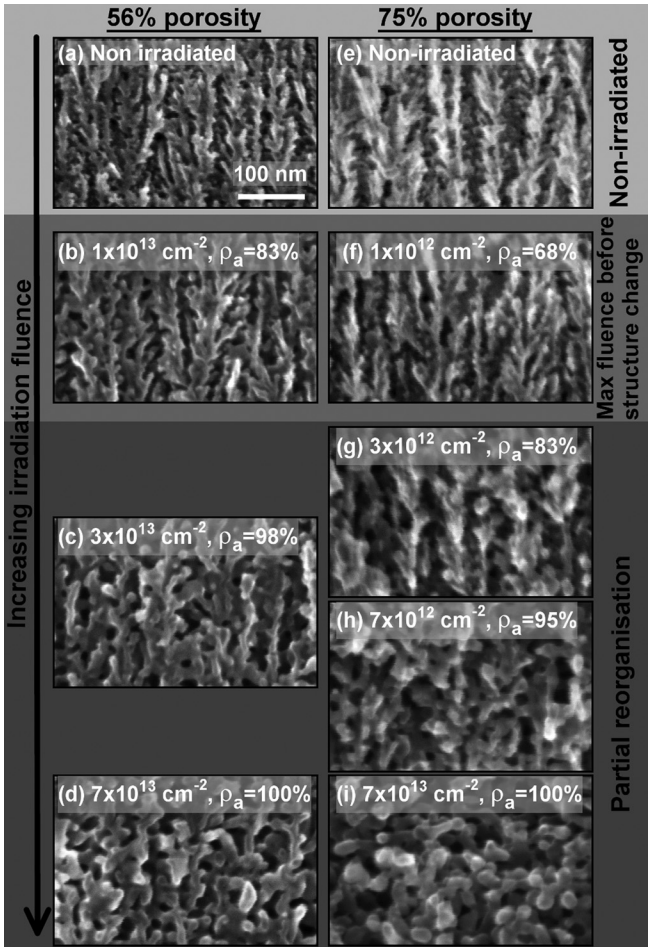

FIG. 4. Cross-section SEM images of 56% and 75% porosity at different irradiation fluences. Irradiation fluence and amorphous volume fraction (ρ_a) are indicated on each image, and all images are at the same magnification.

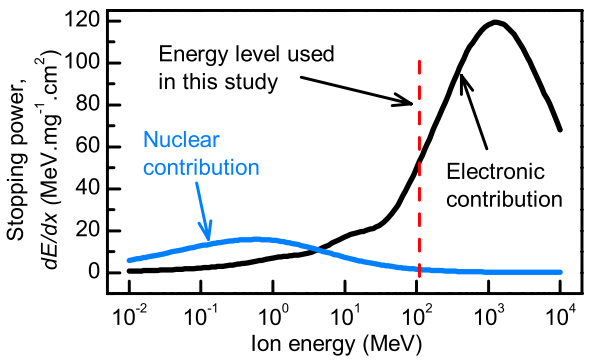

FIG. 5. Nuclear and electronic contributions to stopping power versus ion energy for uranium in silicon. Electronic interactions are dominant at the energy level used in this study (110 MeV).

the introduction that bulk crystalline silicon is insensitive to electronic regime damage caused by irradiation with single ion species. What makes amorphization of porous silicon possible, at energy-density levels which have no effect on bulk crystalline silicon? Damage creation in the electronic regime is commonly described by the thermal spike model,[32] whereby the target electrons, previously excited by the incoming ions in the first 10^{-15} s following their passage, transfer their energy to the crystal lattice via electron-phonon coupling (10^{-12} s). This in turn can cause the target to melt locally, if the deposited energy density is high enough. Although the mechanisms describing electronic-regime interactions in crystalline silicon are not fully understood,[33,34] the thermal spike model can still be applied at least qualitatively.[17] To date, the only known method for creating amorphous tracks in bulk c-Si is with fullerenes,[19] which have a much higher electronic stopping power than uranium and other single ions.[34] In the case of PSi, it is possible that its structure (silicon quasi-columns, with a diameter on the order of 10 nm, surrounded by voids) causes electronic confinement, which could help the deposited energy density reach levels high enough to amorphize silicon. This also explains why high-porosity porous silicon is more sensitive to irradiation, and a higher degree of amorphization can be reached for a given fluence. Indeed, the diameter of the PSi quasi-columns decreases as porosity becomes higher, thus further increasing the energy density.

IV. IMPACT ON THERMAL CONDUCTIVITY

A. Experimental results

Figure 6 shows the thermal conductivity of PSi versus amorphous fraction, as measured by SThM (41% porosity) and Raman spectroscopy (41%, 56%, and 75% porosity). The experimental results are also compared to a simple model, details of which are given below. We can observe that an increase in amorphous fraction caused a reduction of thermal conductivity for all porosities. The model data also displayed similar trends. At 41% porosity, there is a good agreement between the SThM and Raman measurements. The reduction of thermal conductivity reached a factor of up to 3 for 56% porosity and a fluence of $1 \times 10^{13}\,\mathrm{cm}^{-2}$ ($\rho_a = 83\%$), i.e., a reduction from $3\,\mathrm{W\,m^{-1}\,K^{-1}}$ to $0.9\,\mathrm{W\,m^{-1}\,K^{-1}}$. The lowest thermal conductivity measured was $0.5\,\mathrm{W\,m^{-1}\,K^{-1}}$ for 75% porosity PSi at $\rho_a = 68\%$. Furthermore, the 56% porosity sample partially amorphized at $\rho_a = 83\%$ had a slightly lower thermal conductivity than the non-irradiated 75% porosity sample ($0.9\,\mathrm{W\,m^{-1}\,K^{-1}}$ versus $1.1\,\mathrm{W\,m^{-1}\,K^{-1}}$). Therefore, by irradiating and amorphizing medium porosity samples, we were able to obtain lower thermal conductivities than high porosity samples, thus avoiding the issues caused by the fragility of high porosity samples.

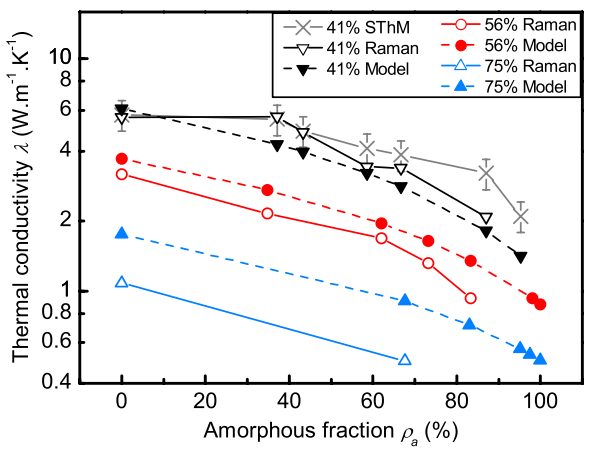

FIG. 6. Thermal conductivity versus amorphous fraction measured by Raman spectroscopy, SThM, and compared to a simple model for different porosities. All data show a decrease in thermal conductivity as amorphous fraction rises.

The thermal conductivity values calculated from the Raman measurements, following the procedure detailed in Appendix B, show a good agreement with the SThM measurements (for 41%) and also with typical values from the literature,[2,3,35,36] thus confirming the validity of this procedure. The thickness of the PSi samples does not affect our SThM results, as this technique probes a depth of around 1 μm.[35]

The irradiated and non-irradiated reference samples were anodised at the same time and stored under room temperature and atmosphere for over a year after the irradiation experiments, before carrying out the thermal conductivity measurements. Room-temperature oxidation is expected, but the thermal conductivity measurements were performed simultaneously on the non-irradiated and irradiated samples, thus eliminating the effect of room-temperature oxidation. Therefore, the reduction in thermal conductivity we measured is only due to amorphization.

B. Discussion on the impact of amorphization on thermal conductivity

We can conclude from these results that the irradiation-induced appearance of the amorphous phase in the PSi layers is responsible for the important decrease in thermal conductivity. As λ for a-Si is lower than that of the PSi nanostructures, the introduction of an amorphous phase reduces the effective thermal conductivity of the whole meso-porous layer. Indeed, assuming a parallel-wire configuration of the amorphous and crystalline phases, the cross-plane thermal conductivity of a partially amorphized PSi layer can be estimated from the following equation:

$$\lambda_{PSi} = (1 - P)[\lambda_{Si}(1 - \rho_a) + \lambda_{aSi}\rho_a],$$

where P is the porosity, and λ_{PSi}, λ_{Si}, and λ_{aSi} are the thermal conductivity of, respectively, the PSi layer, crystalline Si nanowires, and a-Si. The parallel wire assumption is reasonable and is based on the fact that there is no significant Raman shift of the c-Si peak between the non-irradiated and irradiated spectra, as can be seen in Fig. 1. The position of this peak depends on several factors, in particular stress[37] and the characteristic dimension of the PSi nanostructures.[38,39] Therefore, we assume

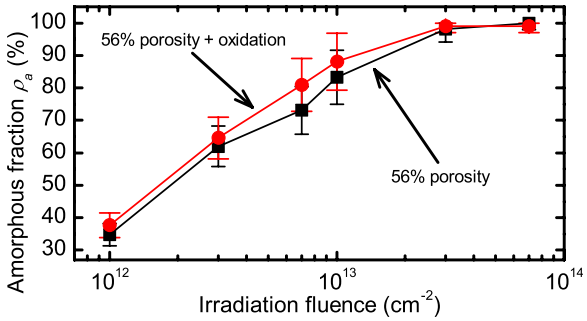

FIG. 7. Amorphous fraction versus irradiation fluence for non-oxidised and oxidised 56% porosity PSi as measured by Raman spectroscopy. The results for non-oxidised 56% PSi are repeated here for comparison with the oxidised results. Oxidation has a low impact on amorphization.

that the diameter of the nanowires that remain crystalline does not change and that the nanowires crossed by an ion become totally amorphous. This, of course, is only valid insofar as the material maintains its porous structure. The thermal conductivity of the crystalline Si nanowires constituting the PSi can be obtained from the model proposed by Chantrenne *et al.*[40] Indeed, this model predicted the thermal conductivity of nanowires with a diameter down to 22 nm and was successfully validated by experimental data.[41,42] The diameter of the PSi nanowires is calculated from the position of the c-Si peak of the non-irradiated PSi spectra[39] and is between 7 and 14 nm, depending on porosity. The thermal conductivity values of the PSi nanowires were found by extrapolating this model to our case. Thermal conductivity values of a-Si vary in the literature between 1 and 5 $W\,m^{-1}\,K^{-1}$,[14] so an intermediate value of $\lambda_{aSi} = 2\,W\,m^{-1}\,K^{-1}$ was chosen for our model. Values of λ_{PSi} calculated with this simple model are plotted in Fig. 6 and compared to the experimental results. The impact of amorphization on the reduction of thermal conductivity is well captured by this simple representation, which confirms that the introduction of an amorphous phase leads to a decrease in thermal conductivity. The model could be refined by taking into account the surface state of the PSi nanowires and its variable cross-section, as both these factors have been shown to affect the thermal conductivity of silicon nanowires.[43–45]

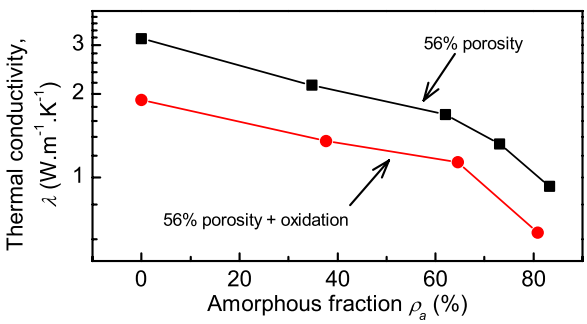

FIG. 8. Thermal conductivity versus amorphous fraction for non-oxidised and oxidised 56% porosity PSi as measured by Raman spectroscopy. The results for non-oxidised 56% PSi are repeated here for comparison with the oxidised results. The thermal conductivity of pre-oxidised PSi is lower than that of non-oxidised PSi.

C. Combined effect of oxidation and amorphization on the thermal conductivity of porous silicon

As mentioned earlier, it has been demonstrated that a thin layer of SiO_2 can reduce the thermal conductivity of PSi by up to a factor of two. Therefore, we oxidised some 56% porosity PSi samples at 300 °C for an hour, before irradiating them. The graph in Fig. 7 shows that the amorphous fraction of oxidised PSi is slightly higher than that of non-oxidised PSi with the same porosity, but otherwise follows the same trend. However, as illustrated by Fig. 8, at a given oxidised fraction ρ_a, the thermal conductivity of PSi is consistently lower after oxidation, and the lowest value obtained is $\lambda = 0.6\,W\,m^{-1}\,K^{-1}$ for $\rho_a = 81\%$. This amounts to a reduction by a factor of five compared to the thermal conductivity of PSi before oxidation and irradiation, so oxidation and irradiation can be combined to maximise the decrease in thermal conductivity.

V. CONCLUSIONS

We have shown that swift heavy ion irradiation with 110 MeV uranium ions can create an amorphous phase in porous silicon, which also results in a considerable reduction of PSi thermal conductivity. Despite high amorphization, PSi remains porous, with only partial reorganisation of its structure for very high amorphization levels. Both the amorphous volume fraction and thermal conductivity can be controlled with the irradiation fluence. For 56% porosity and a fluence of $1 \times 10^{13}\,cm^{-2}$, thermal conductivity was reduced by a factor of 3. Furthermore, we were able to reduce the thermal conductivity of medium porosity samples to levels lower than that of non-irradiated samples of high porosity, thus preventing problems associated with the mechanical stability of high porosity samples. As such, swift heavy ion irradiation is an effective method for improving the thermal insulation properties of PSi layers. It can also be combined with low-temperature oxidation of PSi to further reduce its thermal conductivity.

These results are also significant from a fundamental point of view, as we have demonstrated that in this case, silicon amorphization is caused by electronic-regime interactions, which until now had never been achieved in crystalline silicon with single ion species.

Finally, this technique could have applications as a method for fabricating thick amorphous silicon layers. In the future, we will attempt to obtain the same effect with lower energies to make this technique practical in large-scale applications. Furthermore, the long-term stability of the irradiated samples will be assessed, as well as their mechanical resistance.

ACKNOWLEDGMENTS

The authors are indebted to Professor Vincent Aimez for helping to make this project possible. They also wish to thank Professor Bernard Champagnon and the staff of the CECOMO for assistance with the Raman measurements, the GANIL for the irradiation experiments, and Dmitry Andrusenko for fruitful discussions. They are grateful to NSERC, NanoQuébec, and the Rhône-Alpes region for financial support.

APPENDIX A: MEASUREMENT OF THE AMORPHOUS VOLUME FRACTION FROM THE RAMAN SPECTRA

Calculating the amorphous volume fraction using the Raman spectra of irradiated PSi is a three step process: (i) the spectrum of non-irradiated PSi is fitted, which is then used to (ii) separate the c-Si and a-Si phases, and (iii) the relative integrated areas of these two phases are used to calculate their volume fractions.

Figure 9 compares a Raman spectrum typical of non-irradiated PSi with that of crystalline silicon (inset): the PSi peak is shifted by a few cm^{-1} and asymmetrically broadened, both towards lower energies. These changes are usually ascribed to phonon confinement.[38,39] This increases with porosity, and in high porosity samples, a low-energy tail around $480\,cm^{-1}$ is also present.[46] Therefore, we fitted the non-irradiated PSi spectra with four Gaussian curves: one around $520\,cm^{-1}$ for the c-Si TO phonon, two free between 490 and $520\,cm^{-1}$ for the phonon confinement effects, and one peak at $480\,cm^{-1}$ to fit the low energy tail. Note that the $480\,cm^{-1}$ peak present initially in non-irradiated PSi due to the low energy tail of the spectrum was included in the non-irradiated PSi contribution. Therefore, the amorphous volume fraction calculated is only the amorphous phase created by irradiation.

To separate the c-Si phase and the a-Si phase created by irradiation, we subtracted the crystalline PSi phase from this spectrum by fitting it with a scaled non-irradiated PSi curve and a Gaussian curve at $480\,cm^{-1}$ (characteristic of amorphous silicon). An example is shown in Fig. 2 for the spectrum of a 56% PSi sample which contains an amorphous phase created by irradiation. The fitting procedure for both non-irradiated and irradiated samples was carried out on the portion of the spectra between 400 and $570\,cm^{-1}$, and the baseline was assumed to be linear and subtracted during the fitting procedure.

The amorphous fraction is calculated using $\rho_a = yI_a/(I_c + yI_a)$,[47] where $y = \Sigma_c/\Sigma_a$[48] is the ratio of the Raman cross-sections of a-Si and c-Si, and I_c and I_a are the integrated intensities of, respectively, the c-Si and a-Si phases. The correct value for y is still debated in the literature,[49] with values anywhere between 0.1 and 1.7 having been published,[47–52] and even the validity of this technique has been questioned.[53] The aim of this article is not to shed light on this question, we only wish to extract quantitative information on amorphization we have observed, so we shall simply use the ratio of integrated intensities $\rho'_a = I_a/(I_c + I_a)$ to estimate the amorphous volume fraction ρ_a (i.e., y = 1).

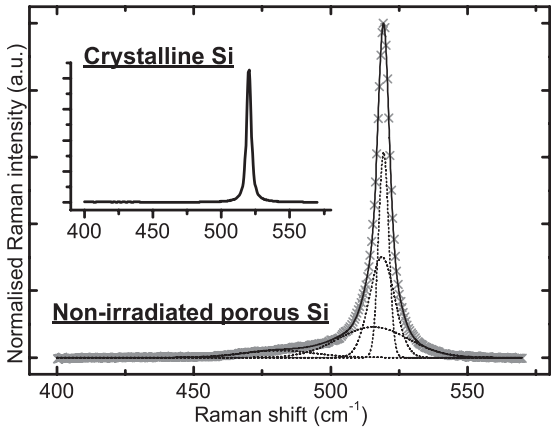

FIG. 9. Fitting procedure of non-irradiated porous silicon (here 56% porosity): the experimental spectrum (crosses) is fitted with four Gaussian curves (dotted lines), to obtain a fitted spectrum (solid line). Inset: a typical spectrum of crystalline silicon is given for comparison.

APPENDIX B: MEASUREMENT OF THERMAL CONDUCTIVITY BY RAMAN SPECTROSCOPY: CORRECTION FOR FINITE THICKNESS OF POROUS SILICON LAYER

The modelled geometry is illustrated in Fig. 10. The porous Si layer has a thickness of $d = 10\,\mu m$ on top of a substrate of bulk c-Si. The thermal conductivities of the two layers are, respectively, λ_{PSi} and λ_{c-Si}. The laser used for the Raman measurements is described as a Gaussian beam with an exponential decay in depth of the power absorbed by unit volume, G[54]

$$G = \frac{2P_0}{\pi b^2}\alpha \exp(-\alpha z)\exp\left(-\frac{2r^2}{b^2}\right), \tag{B1}$$

where P_0 is the total power absorbed by the sample, b the radius of the laser beam, and α the absorption coefficient, while z and r are the cylindrical coordinates. We assume that all the laser power is absorbed by the PSi layer, which is reasonable given that the optical penetration depth is on the order of $1\,\mu m$ for PSi.[55] The values used for α were 9700, 8300, and $5900\,cm^{-1}$ for, respectively, 41%, 56%, and 75% porosity PSi.[56] We wish to calculate the temperature elevation caused by laser heating T, defined as the difference between the sample temperature and ambient temperature. The heating caused by the axi-symmetric laser beam can be described by the 2D heat diffusion equation in cylindrical coordinates,

$$\begin{cases} \dfrac{\lambda_{PSi}}{r}\dfrac{\partial}{\partial r}\left(r\dfrac{\partial T}{\partial r}\right) + \lambda_{PSi}\dfrac{\partial^2 T}{\partial z^2} = -\dfrac{2P_0}{\pi b^2}\alpha \exp(-\alpha z)\exp\left(-\dfrac{2r^2}{b^2}\right) & \text{if } 0 < z < d \\ \dfrac{\lambda_{c-Si}}{r}\dfrac{\partial}{\partial r}\left(r\dfrac{\partial T}{\partial r}\right) + \lambda_{c-Si}\dfrac{\partial^2 T}{\partial z^2} = 0 & \text{if } d < z. \end{cases} \tag{B2}$$

The surface temperature for a given laser power can be calculated from the corresponding measured Raman shift, using a factor of $-0.025\,cm^{-1}\,^{\circ}C^{-1}$.[29] Continuity of temperature and heat flux at the boundary between the PSi layer and c-Si substrate is ensured by

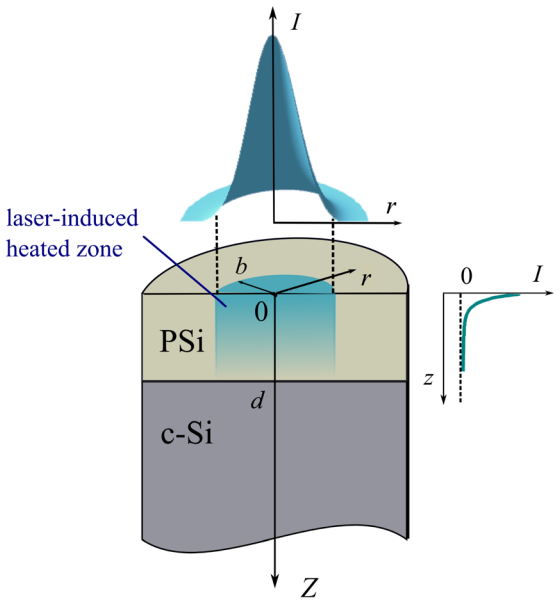

FIG. 10. Geometry used to model the laser-induced heating during thermal conductivity measurements by Raman spectroscopy.

$$\begin{cases} T|_{z=d^-} = T|_{z=d^+} \\ \lambda_{PSi}\dfrac{\partial T}{\partial z}\bigg|_{z=d^-} = \lambda_{c-Si}\dfrac{\partial T}{\partial z}\bigg|_{z=d^+}. \end{cases} \tag{B3}$$

The boundary conditions are zero heat flux from the PSi surface and no temperature elevation at an infinite distance from the sample surface

$$\begin{cases} \dfrac{\partial T}{\partial z}\bigg|_{z=0} = 0 \\ T|_{z\to+\infty}. \end{cases} \tag{B4}$$

The solution to this equation can be found using the methods exposed by Tikhonov and Samarskii[57] and is in the following form:

$$T(r,z) = \sum_{n=1}^{\infty} Z_n(z) J_0\left(\frac{\mu_n^{(0)} r}{R}\right), \tag{B5}$$

where J_0 is a zero-order Bessel function of the first kind, μ_n its n-th root, R the effective sample radius, and Z_n the coefficients of the Fourier-Bessel series. These coefficients depend on z and they can be found by substituting Eq. (B5) into Eqs. (B2)–(B4). In our assumption R is large enough so that there is no temperature increase (this is a good approximation for $R > 400\,\mu$m).

[1]C. J. Glassbrenner and G. A. Slack, Phys. Rev. **134**, A1058 (1964).
[2]G. Gesele, J. Linsmeier, V. Drach, J. Fricke, and R. Arens-Fischer, J. Phys. D **30**, 2911 (1997).
[3]V. Lysenko, S. Perichon, B. Remaki, and D. Barbier, Sens. Actuators, A **99**, 13 (2002).
[4]S.-M. M. Lee and D. G. Cahill, J. Appl. Phys. **81**, 2590 (1997).
[5]G. Kaltsas and A. G. Nassiopoulou, Sens. Actuators, A **76**, 133 (1999).
[6]C. Populaire, B. Remaki, V. Lysenko, D. Barbier, H. Artmann, and T. Pannek, Appl. Phys. Lett. **83**, 1370 (2003).
[7]S. P. Duttagupta, X. L. Chen, S. A. Jenekhe, and P. M. Fauchet, Solid State Commun. **101**, 33 (1997).
[8]U. Grüning and A. Yelon, Thin Solid Films **255**, 135 (1995).
[9]S. Périchon, V. Lysenko, P. Roussel, B. Remaki, B. Champagnon, D. Barbier, and P. Pinard, Sens. Actuators, A **85**, 335 (2000).
[10]V. Lysenko, S. Perichon, B. Remaki, D. Barbier, and B. Champagnon, J. Appl. Phys. **86**, 6841 (1999).
[11]K. Imai and H. Unno, IEEE Trans. Electron Devices **31**, 297 (1984).
[12]K. Barla, R. Herino, and G. Bomchil, J. Appl. Phys. **59**, 439 (1986).
[13]D. G. Cahill, S. K. Watson, and R. O. Pohl, Phys. Rev. B **46**, 6131 (1992).
[14]Y. He, D. Donadio, and G. Galli, Appl. Phys. Lett. **98**, 144101 (2011).
[15]M. Nastasi, J. Mayer, and J. K. Hirvonen, *Ion-Solid Interactions: Fundamentals and Applications* (Cambridge University Press, Cambridge, 1996), p. 572.
[16]A. Simon, F. Pászti, A. Manuaba, and A. Z. Kiss, Nucl. Instrum. Methods Phys. Res. B **158**, 658 (1999).
[17]W. Wesch, A. Kamarou, and E. Wendler, Nucl. Instrum. Methods Phys. Res. B **225**, 111 (2004).
[18]N. Itoh, D. M. Duffy, S. Khakshouri, and A. M. Stoneham, J. Phys: Condens. Matter **21**, 474205 (2009).
[19]B. Canut, N. Bonardi, S. M. M. Ramos, and S. Della-Negra, Nucl. Instrum. Methods Phys. Res. B **146**, 296 (1998).
[20]T. M. Bhave, S. V. Bhoraskar, S. Kulkarni, and V. N. Bhoraskar, J. Phys. D **29**, 462 (1996).
[21]K. Sehrawat, F. Singh, B. P. Singh, and R. M. Mehra, J. Lumin. **106**, 21 (2004).
[22]L. G. Jacobsohn, B. L. Bennett, D. W. Cooke, R. E. Muenchausen, and M. Nastasi, J. Appl. Phys. **97**, 033528 (2005).
[23]W. H. Lee, C. Lee, and J. Jang, J. Non-Cryst. Solids **198–200**, 911 (1996).
[24]S. Billat, M. Thönissen, R. Arens-Fischer, M. G. Berger, M. Krüger, and H. Lüth, Thin Solid Films **297**, 22 (1997).
[25]M. J. Sailor, *Porous Silicon in Practice*, 1st ed. (Wiley-VCH, Weinheim, 2012), p. 250.
[26]See www.ganil-spiral2.eu for Grand Accélérateur National d'Ions Lourds, Caen, France.
[27]S. Gomès, P. Newby, B. Canut, K. Termentzidis, O. Marty, L. Fréchette, P. Chantrenne, V. Aimez, J.-M. Bluet, and V. Lysenko, Microelectron. J. (to be published), doi: 10.1016/j.mejo.2012.07.006.
[28]S. Périchon, V. Lysenko, B. Remaki, D. Barbier, and B. Champagnon, J. Appl. Phys. **86**, 4700 (1999).
[29]C. Populaire, "Propriétés physiques du silicium poreux: Traitements et applications aux microsystèmes," Ph.D. dissertation, INSA Lyon (2005).
[30]J. E. Smith, Jr., M. H. Brodsky, B. L. Crowder, and M. I. Nathan, Phys. Rev. Lett. **26**, 642 (1971).
[31]J. F. Ziegler, M. D. Ziegler, and J. P. Biersack, Nucl. Instrum. Methods Phys. Res. B **268**, 1818 (2010).
[32]M. Toulemonde, C. Dufour, and E. Paumier, Phys. Rev. B **46**, 14362 (1992).
[33]O. Osmani, I. Alzaher, T. Peters, B. Ban d'Etat, A. Cassimi, H. Lebius, I. Monnet, N. Medvedev, B. Rethfeld, and M. Schleberger, Nucl. Instrum. Methods Phys. Res. B **282**, 43 (2012).
[34]M. Murat, A. Akkerman, and J. Barak, Nucl. Instrum. Methods Phys. Res. B **269**, 2649 (2011).
[35]S. Gomès, L. David, V. Lysenko, A. Descamps, T. Nychyporuk, and M. Raynaud, J. Phys. D **40**, 6677 (2007).
[36]G. Amato, R. Angelucci, G. Benedetto, L. Boarino, L. Dori, P. Maccagnani, A. M. Rossi, and R. Spagnolo, J. Porous Mater. **7**, 183 (2000).
[37]O. Marty, T. Nychyporuk, J. de La Torre, V. Lysenko, G. Bremond, and D. Barbier, Appl. Phys. Lett. **88**, 101909 (2006).
[38]H. Richter, Z. P. Wang, and L. Ley, Solid State Commun. **39**, 625 (1981).
[39]I. H. Campbell and P. M. Fauchet, Solid State Commun. **58**, 739 (1986).
[40]P. Chantrenne, J. L. Barrat, X. Blase, and J. D. Gale, J. Appl. Phys. **97**, 104318 (2005).
[41]D. Li, Y. Wu, P. Kim, L. Shi, P. Yang, and A. Majumdar, Appl. Phys. Lett. **83**, 2934 (2003).
[42]M. Asheghi, M. N. Touzelbaev, K. E. Goodson, Y. K. Leung, and S. S. Wong, J. Heat Transfer **120**, 30 (1998).
[43]A. I. Hochbaum, R. Chen, R. D. Delgado, W. Liang, E. C. Garnett, M. Najarian, A. Majumdar, and P. Yang, Nature **451**, 163 (2008).
[44]D. L. Nika, A. I. Cocemasov, C. I. Isacova, A. A. Balandin, V. M. Fomin, and O. G. Schmidt, Phys. Rev. B **85**, 205439 (2012).
[45]X. Zianni and P. Chantrenne, J. Electron. Mater. **42**(7), 1509–1513 (2013).
[46]I. Gregora, B. Champagnon, and A. Halimaoui, J. Appl. Phys. **75**, 3034 (1994).

[47]E. Bustarret, M. A. Hachicha, and M. Brunel, Appl. Phys. Lett. **52**, 1675 (1988).
[48]R. Tsu, J. Gonzalez-Hernandez, S. S. Chao, S. C. Lee, and K. Tanaka, Appl. Phys. Lett. **40**, 534 (1982).
[49]E. Vallat-Sauvain, C. Droz, F. Meillaud, J. Bailat, A. Shah, and C. Ballif, J. Non-Cryst. Solids **352**, 1200 (2006).
[50]C. Smit, R. A. C. M. M. van Swaaij, H. Donker, A. M. H. N. Petit, W. M. M. Kessels, and M. C. M. van de Sanden, J. Appl. Phys. **94**, 3582 (2003).
[51]D. Han, J. D. Lorentzen, J. Weinberg-Wolf, L. E. McNeil, and Q. Wang, J. Appl. Phys. **94**, 2930 (2003).
[52]M. Ledinský, A. Vetushka, J. Stuchlík, T. Mates, A. Fejfar, J. Kočka, and J. Štěpánek, J. Non-Cryst. Solids **354**, 2253 (2008).
[53]C. Ossadnik, S. Vepek, and I. Gregora, Thin Solid Films **337**, 148 (1999).
[54]M. Lax, J. Appl. Phys. **48**, 3919 (1977).
[55]D. Andrusenko, M. Isaiev, A. Kuzmich, V. Lysenko, and R. Burbelo, Nanoscale Res. Lett. **7**, 411 (2012).
[56]J. von Behren and P. M. Fauchet, *in Properties of Porous Silicon*, edited by L. Canham (The IEE, London, 2006) 1st ed., Chap. 8.2, p. 405.
[57]A. N. Tikhonov and A. A. Samarskii, *Equations of Mathematical Physics*, 1st ed. (Dover Publications, 2011), p. 800.